Physica Scripta

PAPER

Computer simulation of phosphate-silicate and calcium phosphate-silicate systems

To cite this article: Nguyen Van Hong *et al* 2023 *Phys. Scr.* **98** 065704

IOP Publishing Phys. Scr. 98 (2023) 065704 https://doi.org/10.1088/1402-4896/acd4fb

Physica Scripta

RECEIVED
26 January 2023

REVISED
28 April 2023

ACCEPTED FOR PUBLICATION
12 May 2023

PUBLISHED
24 May 2023

PAPER

Computer simulation of phosphate-silicate and calcium phosphate-silicate systems

Nguyen Van Hong[1,*], **Nguyen Hoang Anh**[1], **Toshiaki Iitaka**[2] and **Mai Thi Lan**[1]

[1] Hanoi University of science and technology, No.1 Dai Co Viet, Hanoi, Vietnam
[2] Discrete Event Simulation Research Team, RIKEN Center for Computational Science (W-B21) 2-1 Hirosawa, Wako, Saitama, 351-0198, Japan
[*] Author to whom any correspondence should be addressed.

E-mail: hong.nguyenvan@hust.edu.vn

Keywords: diffusion mechanism, local structure, network forming liquid, abnormal diffusion

Abstract

The structure of P_2O_5-SiO_2 and CaO-P_2O_5-SiO_2 systems have been systematically investigated by molecular dynamics simulation. The structural characteristics were clarified with intuitive figures and images at atomic scale. Specially, we have applied the recognition and visualization methods to clarify short range order, intermediate range order, and network structure. The structural and compositional heterogeneities and mechanism of alkaline Earth metals incorporation into -O-P-O-Si-O- network have been discussed in detail. This is useful information for designing bioactive systems with many potential applications.

1. Introduction

Glassy network structure of P_2O_5- and SiO_2-based multicomponent oxide systems are at the heart of bioactive glass materials. This material group has been widely investigated for restorative biomedical applications. Their network structure was described as continuous random networks made up of corner-shared glass former-oxide tetrahedra (TO_4 with T = Si, P) with modifier ions in the inter-networking regions. Investigation by both experiment and simulation [1–7] have shown that the distribution of P^{5+} ions in phosphosilicate is in good agreement with statistical distribution within a short-range scale of $\leqslant$450 pm. The P^{5+} ion distribution is independent on the silicate network polymerization and independent on the P content in glass system. Research results in [8–15] shows that the properties of bioactive glasses are strongly dependent on their composition. The bioactive glass containing 55–60 wt% SiO2 required a longer time to bond with bone but did not bond to soft tissue. Meanwhile, silicate glasses with >60 wt% SiO_2 are biologically inert. Report in works [5, 16–21] showed that increasing the P content of Na_2O-CaO-SiO_2-P_2O_5 system will promotes apatite formation. Increasing P_2O_5 content expands the range of silicate network connectivity, which offers a high bioactivity. The bioactivity is strongly dependent on the silicate network connectivity and the number of bridging oxygens (BO). Investigation also revealed a weak relationship between the critical non-bridging oxygens (NBO) value and the P content. Simulation and experimental data in [7, 14, 22–31] revealed that the medium-range order structure is significantly dependent on thermal history of the glass. The authors in work [7] have observed an increased affinity of P atoms toward NBOs that accompanying a decrease in the fraction of Si-O-P bridges upon lower cooling rates. For diopside (CaO.MgO.2SiO_2)- tricalcium phosphate (3CaO.P_2O_5) glass systems, the investigation in [9, 14, 16, 32–40] showed that the glass network structure consists predominantly of Q^2 and Q^3 species (here Q^n is the SiO_x, POx or TOx (T = Si, P) with n bridging oxygens between Si-Si, P-P and T-T, respectively). The amounts of Q^2 decreases as diopside content increases. Meanwhile amounts of Q^3 increases with the increase of diopside content. The glass network connectivity decreases with increasing tricalcium phosphate and P_2O_5 content. In the considered composition, -Si-O-Si-O- network connectivity (NC) remains almost constant, NC is around 2. Molecular dynamics simulation data revealed the glass network structure with broader Q^n distributions for Si and higher Q^1 species for P.

Table 1. BMH potential for CPS system [33].

i-j	A_{ij}(eV)	B_{ij}(1/Å)	C_{ij}(eV Å^6)
Ca-Ca	329171.51	6.25	4.34
Ca-Si	26684.39	6.25	0
Ca-P	164585.76	12.50	0
Ca-O	718088.63	6.06	8.67
Si-Si	2163.18	6.25	0
Si-P	1081.59	12.50	0
Si-O	62,817.23	6.06	0
P-P	0	0	0
P-O	1847.66	3.45	0
O-O	1497594.32	5.88	17.35

Neutron diffraction, X-ray diffraction, EXAFS and NMR experiments have provided valuable information on the short-range order (SRO) structure of cations [15, 17, 19, 20, 41–49]. By using the above experimental methods, it is difficult to clarify the composition-structure-property relationships of multicomponent systems due to the lack of intermediate range order (IRO) and long-range order (LRO) [50].

Simulation methods provide quantitative and qualitative insights at the atomic level that can be used to analyze and clarify the structure as well as composition-structure-properties relationship in complex system. Molecular Dynamics and Monte-Carlo simulation methods have been applied in materials research to elucidate the structure and properties of multicomponent systems. The ab-initio molecular dynamics [51, 52] is high accuracy method but it is rather limited due to high computational cost. The quality of a model is determined by the interatomic potentials. For this aspect, density functional theory (DFT) based on *ab initio* molecular dynamics has an advantage of having accurate interatomic potential in comparison to other method using empirical potentials [53–55]. However, it is limited to systems of modest size. The classical molecular dynamics simulation (MDS) has advantage of low computational cost. The availability of accurate empirical potential makes the MDS more useful. Therefore, the classical MDS is getting more and more widely applied in material research [56–68].

Despite their strategical importance in medicine, the relationship between the structure, composition and activity of bioactive glasses has not been studied in detail [10, 69–76]. The trial-and-error approaches are still the main method to optimize the composition, structure, and activity of bioactive glasses for new applications. This fundamental gap negatively affects further progress, for instance, to make bioactive glasses for specific applications. With the quick develop of information technology (both hardware and software), computer simulation is a useful method to obtain an atomistic view into the structure and bioactive behaviors and it fills the gap in fundamental knowledge. Molecular dynamics (MD) simulation now is one of the most effective methods to clarify structure and properties of bioactive glass at atomic scale. For P_2O_5-SiO_2 and CaO-P_2O_5-SiO_2, many researches have been conducted to clarify the -Si-O-P-O-P-O- network structure. However, the distribution of P^{5+} in the silicate network and the effect of alkali and alkaline Earth metals cations on the network structure and bioactivity of phosphate silicate systems is still in debate [8–14, 24, 33–36, 65, 68, 73].

In this work, MD simulation is used to investigate the structure of P_2O_5-SiO_2 and CaO-P_2O_5-SiO_2 systems. In particularly, the visualization method and recognition technique are applied to clarify the network structure, distribution of Ca^{2+} ions in the -Si-O-P-O-P-O- network and the microphase separation. The role of Ca^{2+} ions in the structure and the relationship between structure and composition are also discussed in detail. These structural data are important bases for designing and manufacturing bioactive materials.

2. Methodology

For investigating the effect of network modifier Ca^{2+} on the structures of phosphate-silicate based glassy network, phosphate-silicate and calcium phosphate-silicate systems were considered in the present study. The models of phosphate-silicate (40 mol% P_2O_5 and 60 mol% SiO_2) and calcium phosphate-silicate (10 mol% CaO, 30 mol% P_2O_5 and 60 mol% SiO_2) were constructed by MDS at 3000 K and ambient pressure. Simulations were carried out using Large-scale Atomic/Molecular Massively Parallel Simulator (LAMMPS) software. The classical MDS has the advantage of being easy to apply and computationally inexpensive. It allows large models to be simulated over long timescales. The disadvantage is the limited accuracy of interatomic potentials. In this work, we used interatomic potentials that was represented by an empirical expression (1) [33, 34, 37].

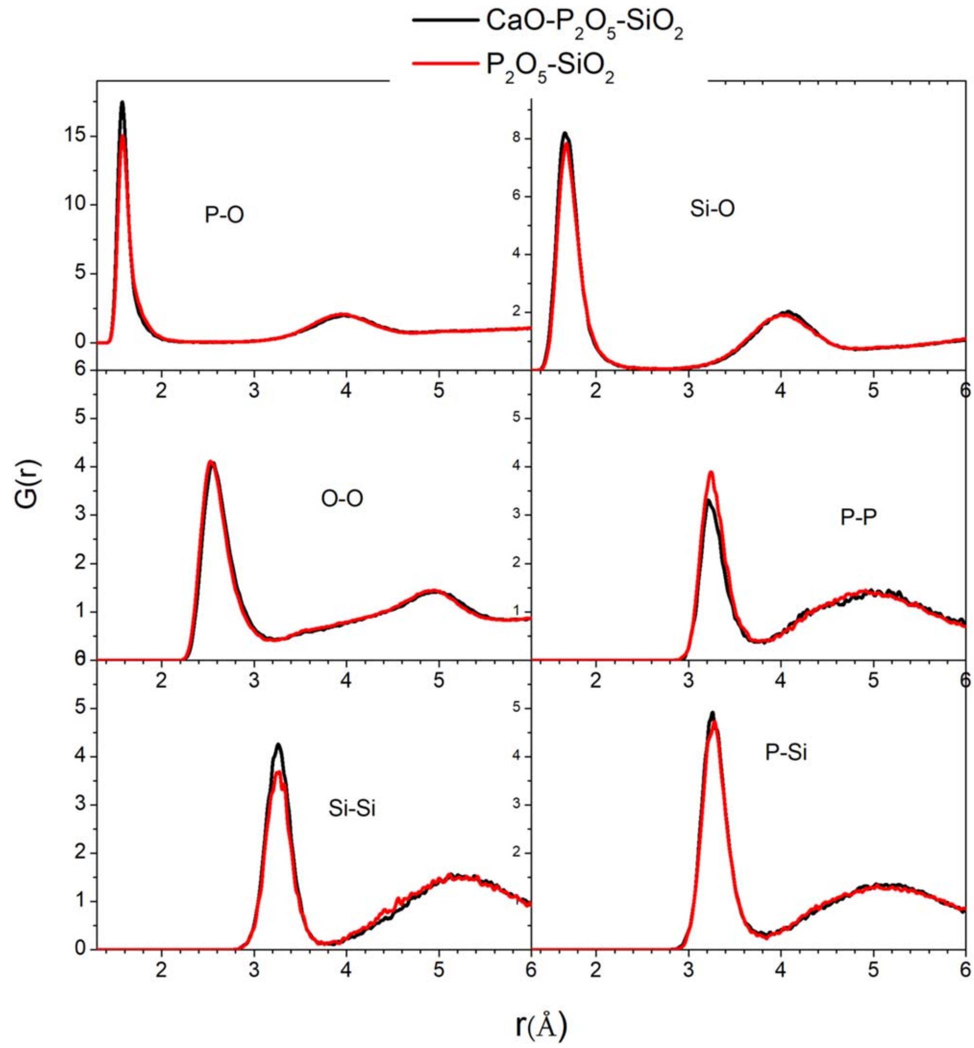

Figure 1. Pair correlation function of atomic pair in P_2O_5-SiO_2 and CaO-P_2O_5-SiO_2 systems.

$$U_{ij} = \frac{q_i q_j}{r_{ij}} + A_{ij}\exp(-B_{ij} r_{ij}) - C_{ij} r_{ij}^{-6} \tag{1}$$

here, $U_{ij}(r)$ is the interatomic potential; q_i and q_j are charges of ions i and j (the charge of Ca, Si, P and O is +2e, +4e, +5e and −2e respectively); r_{ij} is the distance between ions i and j; The potential parameters A_{ij}, B_{ij} and C_{ij} are given in table 1 [33]. The first term on the right-hand side of equation (1) is Coulomb interactions, the second and third terms are short range interactions which include attraction and repulsions between ions. Short range interactions were calculated with cutoff distance of 10 Å. Long range Coulomb interactions were calculated by using the Ewald sum method with a cutoff of 10.0 Å and a relative error in forces of 10^{-4}. The interactions within 10.0 Å are computed directly; interactions outside 10.0 Å are computed in reciprocal space. Simulation is performed using LAMMPS software package (version Lammps-30 Jul 16) with time step of 1.0 fs [77]. The models of 5520 and 5330 atoms corresponding to phosphate-silicate and calcium phosphate-silicate systems were generated by putting randomly atoms into a periodic box. Then, the models were heated up to 5000 K and equilibrated at this temperature to get a properly equilibrated liquid. This ensures that the initial configuration has been removed. Then, these models are cooled down to 3000 K with cooling rate 5 K ps^{-1}. Then, the model was relaxed at 3000 K in NPT ensemble at ambient pressure for 10 ns to get equilibrated state at 3000 K and at ambient pressure. Next, the sample continues to be relaxed in NVE ensemble for a long time (10 ns) to ensure getting equilibrium state (the temperature and pressure of models are 3000 K and ambient pressure, respectively). To calculate the structural characteristics, we used the bond distance of 3.3, 2.1 and 2.4 Å corresponding to Ca-O, P-O, and Si-O pairs. These bond distances were chosen based on the first minimum of the Ca-O, P-O and Si-O RDFs.

In this work, the three-dimensional (3D) visualization techniques have been applied to clarify the -O-P-O-Si-O network structure and distribution of Ca^{2+} ions in CPS and CP system. The algorithm of 3D visualization program is as following: 1/Firstly, the TOx polyhdera (T = P, S) in the model are separated into two different

Table 2. Local structure characteristics of CaO-P_2O_5-SiO_2 and P_2O_5-SiO_2 systems.

	Bond distance(Å)			Bond angle (degree)	
references	Si-O	P-O	Ca-O	O-P-O	O-Si-O
This work	1.6–1.64	1.52–1.56	2.30	110	110
[6]	1.61	1.51	2.37		
[7]	1.6	1.48	2.35	109	109
[9]	1.58–1.62	1.53–1.56	2.28–235		
[10]	1.6	1.60	2.3/255+0.05	107.5	108
[14]	1.6	1.50	2.30		
[16]	1.61	1.60	2.35		
[21]	1.63	1.55	2.32	108.6± 15	107.5± 16
[22]		1.52–1.6	2.29–2.41	107.5–109.0	
[23]	1.625–1.63	3.08–3.16	2.30–2.37		108.4–109.7
[24]	1.6	1.50	2.30		
		1.44–1.66			
[29]		1.53–1.61	2.35		
[30]	1.64–1.66	1.53–1.56	2.46–2.53	109.4	109.3
[33]	1.60–1.61	1.53–1.54	2.30–2.31		
[34]				107.8 ± 18.6	
[35]	1.61	1.53	2.30	109	109.5

Table 3. Intermediate structure characteristics of CaO-P_2O_5-SiO_2 and P_2O_5-SiO_2 systems.

		Interatomic distance (Å)			bond angle (degree)	
references	Si-Si	P-P	P-Si	Si-O-Si	P-O-P	P-O-Si
This work	3.25	3.25	3.25	165	165	165
[7]	3.15		3.1	150		152
10				148	145	149
[14]	3.25	3.25	3.2			
[21]	3.01–3.05			121± 25	124± 20	
[22]		3.05			123.4–132	
[23]				145–156		
[29]						
[30]				144–147		
[33]				131–167	139–175	135–171
[34]					160.3 ± 11.7	

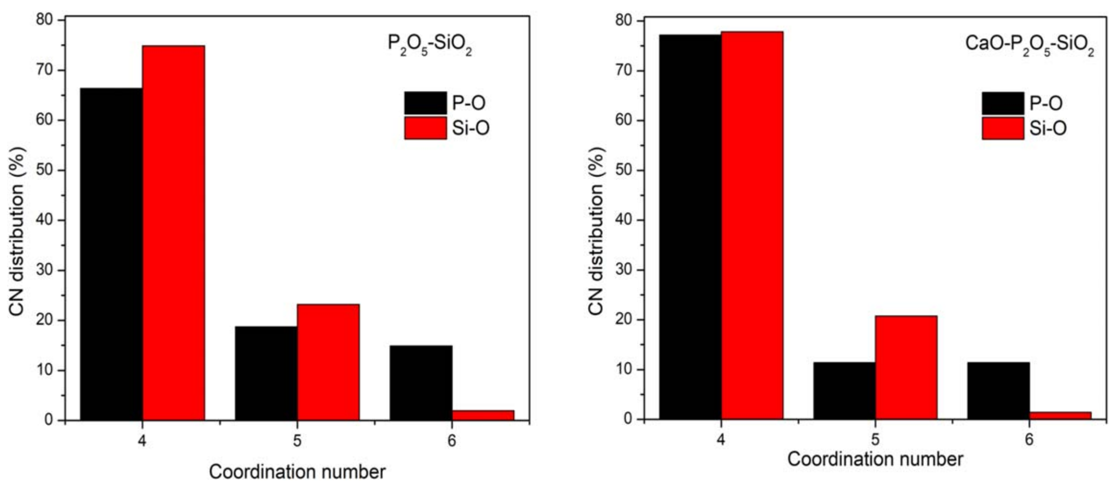

Figure 2. Coordination number distribution of Si-O and P-O pairs in P_2O_5-SiO_2 and CaO-P_2O_5-SiO_2 systems.

Table 4. Distribution of linkages in CaO-P_2O_5-SiO_2 system (10 mol% CaO, 30 mol% P_2O_5 and 60 mol% SiO_2).

Linkage	Distr. (%)	Linkage	Distr. (%)	Linkage	Distr. (%)	Linkage	Distr. (%)
O-P	3.21	Ca-O-P	4.67	P-O-Si	25.74	Ca-O-PSi	3.13
O-P2	4.29	Ca2-O-P	1.48	P-O-Si2	15.58	Ca2-O-PSi	0.85
O-Si2	16.73	Ca3-O-P	0.03	P-O-Si3	5.03	Ca3-O-PSi	0.05
O-Si3	1.98	Ca-O-Si	1.10	P-O-Si4	0.55	Ca-O-P2Si	0.27
O-Si4	0.05	Ca2-O-Si	0.66	P2-O-Si	5.33	Ca-O-PSi2	1.15
		Ca3-O-Si	0.08	P2-O-Si2	3.76	Ca-O-P2Si2	0.14
		Ca-O-P2	0.11	P2-O-Si3	1.51	Ca-O-PSi3	0.25
		Ca-O-Si2	1.43	P-O-Si4	0.55	Ca2-O-PSi2	0.08
		Ca-O-Si3	0.11				
		Ca2-O-Si2	0.08				
Total	26.26	total	9.75	total	58.05	total	5.93

Table 5. Distribution of OB(P) and OB(Si) in CaO-P_2O_5-SiO_2 system (10 mol% CaO, 30 mol% P_2O_5 and 60 mol% SiO_2). Here, OB(P) is bridging oxygen between PO_x and OB(Si) is bridging oxygen between SiO_x.

OB(P)	Distr. (%)	OB(Si)	Distr. (%)
O-P2	4.29	O-Si2	16.73
Ca-O-P2	0.11	O-Si3	1.98
Ca-O-P2Si	0.27	O-Si4	0.05
Ca-O-P2Si2	0.14	P-O-Si2	15.58
P2-O-Si	5.33	P-O-Si3	5.03
P2-O-Si2	3.76	P-O-Si4	0.55
P2-O-Si3	1.51		
Total	15.41	total	39.92

Table 6. Distribution of linkages in P_2O_5-SiO_2 system (40 mol% P_2O_5 and 60 mol% SiO_2).

Linkage	Distr. (%)	Linkage	Distr. (%)	Linkage	Distr. (%)
O-Si	0.31	O-P	4.69	P-O-Si	28.28
O-Si2	13.13	O-P2	5.91	P-O-Si2	17.16
O-Si3	1.59			P2-O-Si	10.05
O-Si4	0.08			P-O-Si3	6.38
				P3-O-Si	0.00
				P2-O-Si2	7.68
				P2-O-Si3	2.92
				P-O-Si4	1.09
				P-O-Si5	0.05
				P2-O-Si4	0.60
				P2-O-Si5	0.08
	15.10		10.60		74.30

sets: SiOx and POx-ones; 2/ the SiOx, POx units and Ca atoms are visualized with different color code. The bonds between Si/P and O atoms in SiOx/POx polyhedra ($x = 4, 5, 6$) are visualized by the cylinders that connects between Si/P and O atoms. The cluster of POx and siOx is highlighted by translucent sphere with high contrast colors.

3. Results and discussion

Firstly, to ensure the reliability of model, the structure characteristics are investigated and compared to the simulation and experiment data in previous works. Figure 1 shows the pair correlation function of P-O, Si-O, O-O, P-P, Si-Si, P-Si pairs. Results show that the P-O and Si-O bond distances are 1.52–1.56 Å and 1.60–1.64 Å, respectively. The P-P, Si-Si and Si-P distances are similar each other and have the value of around 3.25 Å. The P-O and Si-O bond distances characterize the short-range order (SRO) structure that relates to the coordination polyhedral units SiO_4 and PO_4. The P-P, Si-Si and Si-P distances characterize the intermediate range order

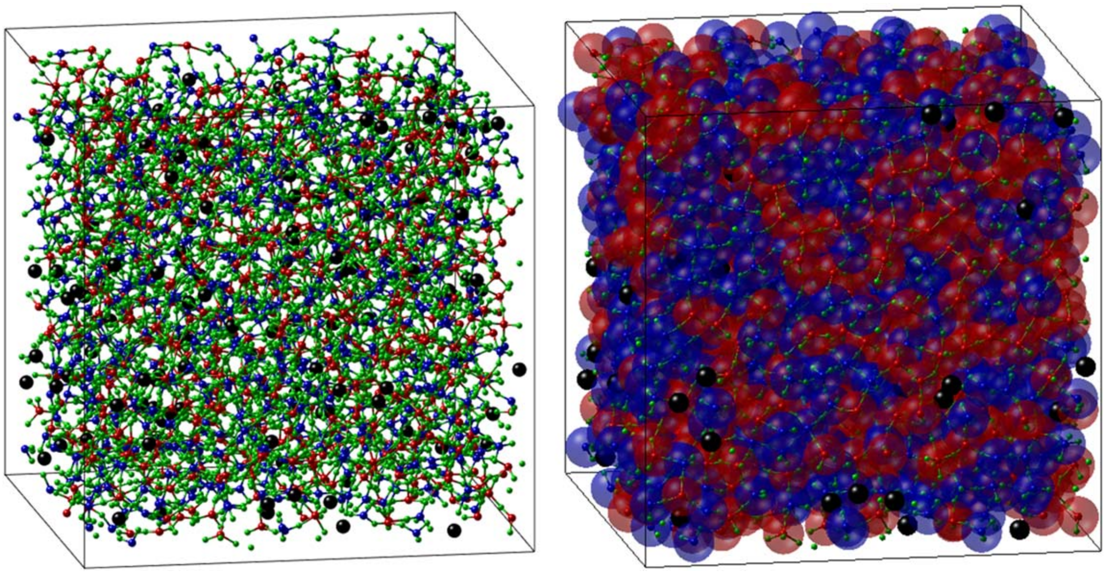

Figure 3. Snapshot of the network structure of CaO-P2O5-SiO2 system: network structure, here Ca in black, Si in red, P in blue, O in green (left); The network structure, in that -P-O-P-O- network is highlighted with blue color, -Si-O-Si-O- network is highlighted with red color (right).

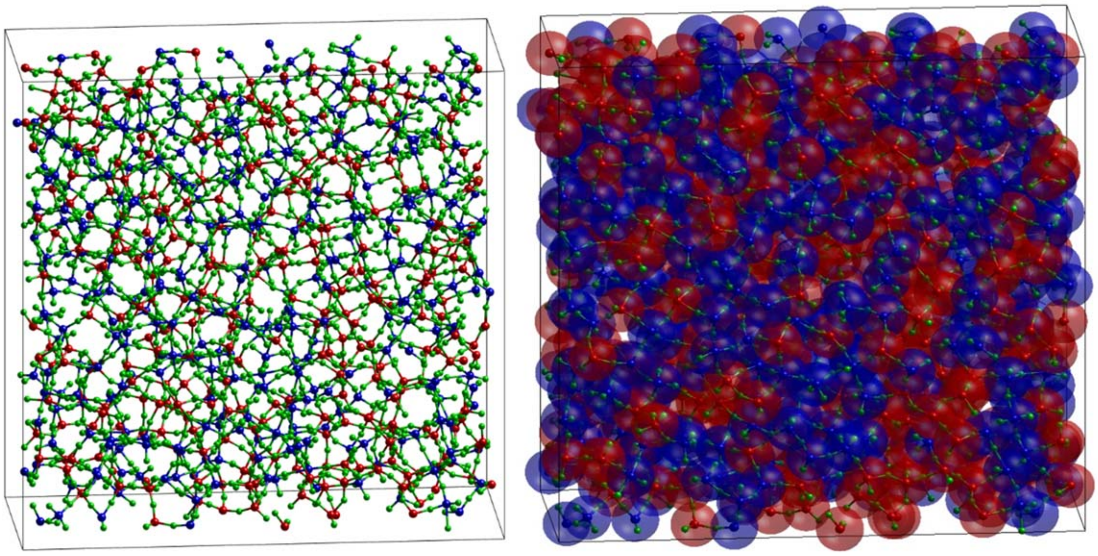

Figure 4. Network structure of CaO-P2O5-SiO2 system removed Ca, here Si in red, P in blue, O in green: The -O-P-O-Si-O- network structure (left); The -O-P-O-Si-O- network structure, in that -P-O-P-O- network is highlighted with blue color, -Si-O-Si-O- network is highlighted with red color (right).

(IRO) that relates to the connection between coordination polyhedral units. The SRO and IRO characteristics such as the bond length distance, coordination number are very slightly dependent on temperature [78–81]. The structural characteristics of PS and CPS in this study are in good agreement with the simulation and experiment data in the works [6, 7, 9, 10, 14, 16, 21–24, 29, 30, 33–35], see tables 2 and 3. Figure 2 shows the coordination number distribution of P-O and Si-O pairs in P_2O_5-SiO_2 and CaO-P_2O_5-SiO_2 systems. It shows that the P^{5+} and Si^{4+} ions can be surrounded by four, five or six O^{2-} cations forming TO_x polyhedra ($T = P$, Si; $x = 4, 5, 6$). Result reveals that most P^{5+} and Si^{4+} ions are surrounded by four O^{2-} cations forming PO_4 and SiO_4 tetrahedral units.

For the P_2O_5-SiO_2 system (called as PS for brief), the concentration of SiO_4, SiO_5, and SiO_6 octahedral units are about 75%, 23% and 2%, respectively. Similarly, the concentration of PO_4, PO_5, and PO_6 octahedral units are about 67%, 18% and 15%, respectively. For CaO-P_2O_5-SiO_2 system (called as CPS for brief), the concentration of SiO_4, SiO_5, and SiO_6 are around 77%, 21% and 2%, respectively. Similarly, the concentration of PO_4, PO_5, and PO_6 are around 77%, 11.5% and 11.5%, respectively. These results reveal that, the coordination number distribution of P-O pair in PS and CPS system is almost the same. However, the

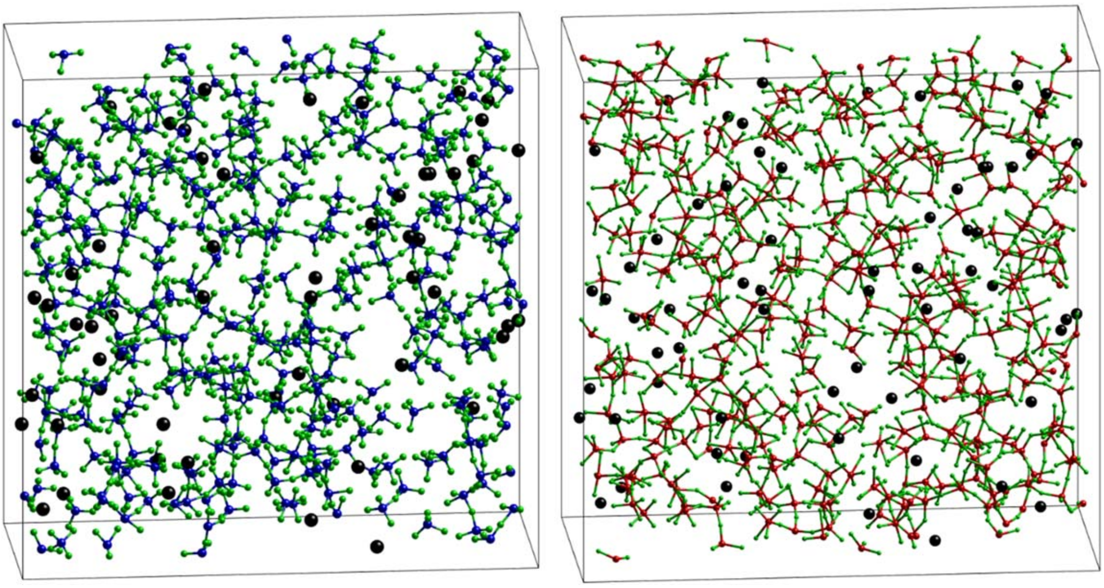

Figure 5. Network structure of CaO-P_2O5-SiO_2 system, here Ca in black, Si in red, P in blue, O in green: The network structure removed Si (left); the network structure removed P(right).

coordination number distribution of Si-O pair in PS and CPS system are significantly different. This means that the Si-O coordination number distribution is significantly affected by CaO content [6, 7, 21, 23].

To clarify the IRO of CPS and PS system, we have investigated the linkage and BO distribution. The investigated results are shown in tables 4, 5 and 6. For CPS, linkages distribution of OT_y (T = Ca, P, Si, y = 1–5) in table 4 reveals that most of Ca^{2+} ions incorporate into -O-P-O-Si-O- network via Non-Bridging Oxygen (NBO) of -O-P-O- network and BO between -O-P-O- network and -O-Si-O- ones. The fraction of O that only links to Ca and P is about 6.22% and they form the Ca-O-P, Ca2-O-P and Ca-O-P2 linkages. The fraction of O forming Ca-O-P, Ca2-O-P and Ca-O-P2 linkages is 4.67%, 1.48% and 0.11%. The fraction of O that only links to Ca and Si is about 3.53%, forming different types of linkages with distribution as following: Ca-O-Si (1.1%), Ca2 -O-Si (0.66%), Ca3-O-Si (0.08%), Ca-O-Si2 (1.43%), Ca-O-Si3 (0.11%) and Ca2-O-Si2 (0.08%). The fraction of the O atoms that only links to P is about 7.5% and they form types of linkages with distribution as following: O-P (3.21%) and O-P2 (4,29%). These linkages form P-rich regions. The O fraction that only links to Si is about 18.76% and forms the types of linkage with distribution as following: O-Si2 (16.73%), O-Si3 (1.98%) and O-Si4 (0.05%). These linkages form the Si-rich regions. The fraction of O that only links to P and Si is about 58%. The fraction of O that links to Ca and both P and Si is about 5.93%, see table 4. The about analysis reveals that distribution of Ca^{2+} ions in -O-P-O-Si-O- network are not uniform. Ca^{2+} ions tend to locate inside -O-P-O– network and at boundary between -O-P-O- and -O-Si-O- networks. This results in forming Ca-rich regions. This indicates the structural and compositional heterogeneities in CPS system [21, 23, 30, 33, 35].

The intuitive data and images about the -O-P-O-Si-O- network as well as the structural and compositional heterogeneities in CPS system are shown in figures 3, 4 and 5. It shows that the network structure of CPS system coexists two types: -O-P-O- and -O-Si-O- networks. Most Ca^{+2} ions distribute in -O-P-O- network. It once again reveals the structural and compositional heterogeneities in CPS system [10, 21, 30, 34]. The structural and dynamical heterogeneities in silicate systems at high temperature also have been reported in work [82–85].

Table 5 shows the distribution of BO(P) and BO(Si), here OB(P) is bridging oxygen between PO_x polyhedral units, and OB(Si) is bridging oxygen between SiO_x polyhedral units. This reveals that the degree of polymerization of -O-Si-O- network is higher than -O-P-O- one. The -O-Si-O- network is the main one in CPS system.

Table 6 shows the distribution of linkages in PS system. Results show that fraction of O that only links to P is about 10.6% meanwhile the fraction of O that only links to Si is about 15.1%. This shows that, the structure of PS system also consists of two types of networks -O-P-O- and -O-Si-O- network. The network structure of PS system is the mixture of the above networks forming P-rich regions besides Si-rich ones, see figure 6.

To clarify more about the network structure of CPS and PS systems, the distribution of Q^n units in CPS and PS systems have been investigated and shown in tables 7 and 8 (here, Q^n is the SiO_x, POx or TO_x (T = Si, P) units with n bridging oxygens between Si-Si, P-P and T-T, respectively). It reveals that most of SiO_x units have one, two or three BOs that link amongst SiO_x. It also exists a lot of isolated SiO_x polyhedral units that have no BO connecting between SiO_x. These isolated SiO_x units only links to Ca or P. In other word, these SiO_x units locates

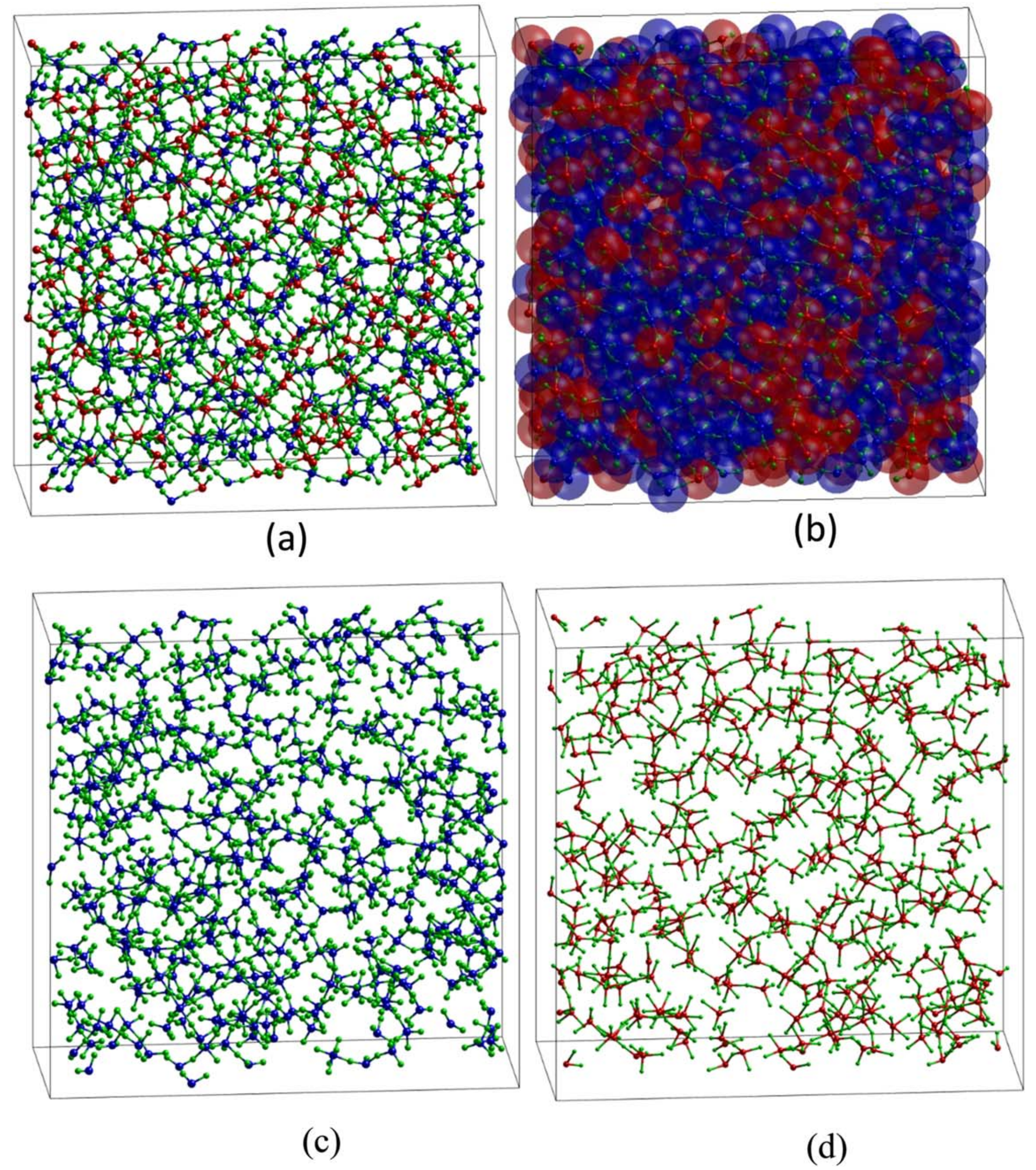

Figure 6. Network structure of P2O5-SiO2 system: the -P-O-Si-O- network (a); The -O-P-O-Si-O- network, in that -P-O-P-O- network is highlighted with blue color, -Si-O-Si-O- network is highlighted with red color (b); the -P-O-P-O- network (c); the -Si-O-Si-O- network (d).

inside -O-P-O- networks. The number of isolated SiO_x consists of 27 SiO_4 units, 21 SiO_5 units and 3 SiO_6 units, see table 7. Most PO_x units have zero, one or two BOs connecting amongst PO_x units. The number of PO_x units have zero, one or two BOs is 184, 273 and 138, respectively. The PO_x units with zero BO is isolated units. These isolated polyhedral units locate inside -O-Si-O- network. Most of TO_x have three, four or five BOs. Results also reveal that most TO_5 units have 4 or 5 BOs. In 243 TO_5 units, the number of TO_5 with 4 BOs and with 5 BO are 36 and 206, respectively. The number of TO_6 units is 89, in that six units with 5 BOs, 83 units with 6 BOs. The distribution of Q^n as well as P^{5+} ions in CPS is especially important in bioactive systems. It determines the dissolution rate of bioactive system in body fluid, or water. The dissolution rate of bioactive material based on CPS system can be controlled and tuned by changing their composition and structure. The P_2O_5 content is a key parameter to control the structure as well as bioactivity of bioactive systemses.

The distribution of Q^n in PS system is shown in table 8. It reveals that most PO_x and SiO_x have zero, one, two or three BOs. Most of SiO_6 are isolated units, or they have only one or two BOs. Meanwhile, most of PO_6 have three, four or five BOs. The number of PO_6 units is large in comparison to the number of SiO_6. Most TO_6 octahedra (T = P, Si) have six BOs. in 139 TO_6 octahedra, there are 136 ones have six BOs (notice: BOs in TOx is the O atoms that connect between P-Si, P-P or Si-Si atoms). Figure 7 show the O-P-O and P-O-P bond angle

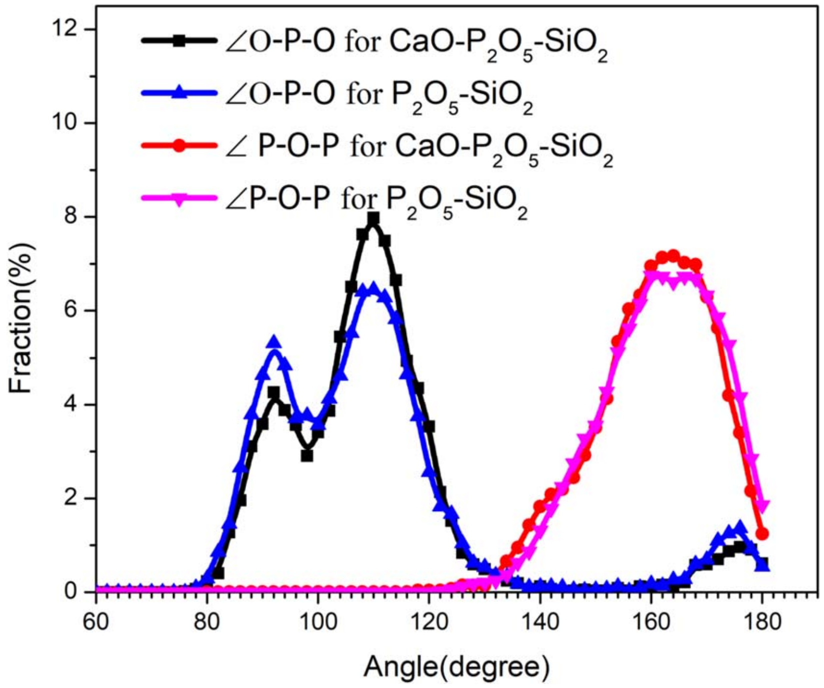

Figure 7. The O-P-O and P-O-P bond angle distribution in P_2O_5-SiO_2 and CaO-P_2O_5-SiO_2 systems.

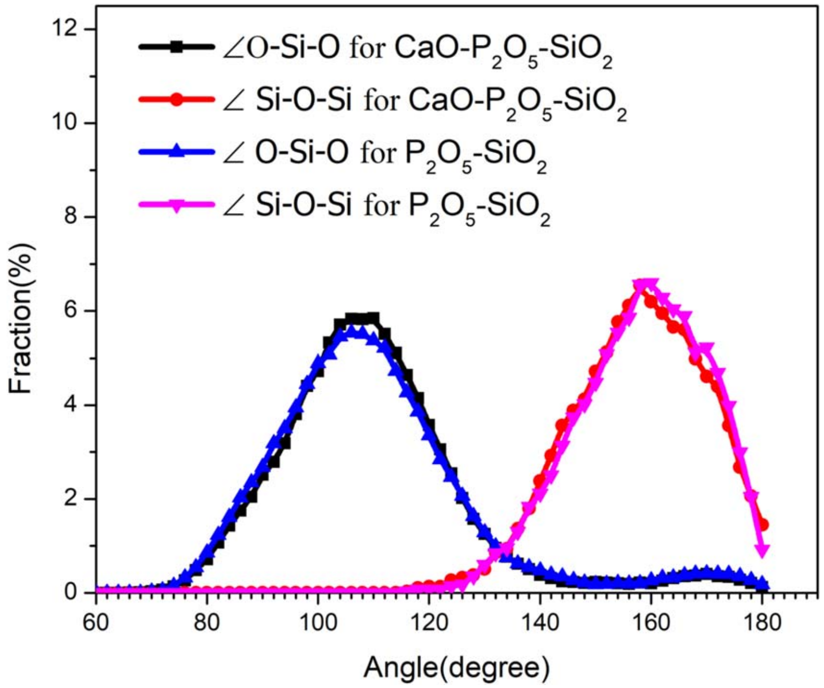

Figure 8. The O-Si-O and Si-O-Si bond angle distribution in P_2O_5-SiO_2 and CaO-P_2O_5-SiO_2 systems.

distribution in PS and CPS systems. Result shows that O-P-O bond angle distribution has three peaks at 92, 110 and 175° corresponding to angle in pentahedra, tetrahedra and octahedra. The peak at 92 and 175° for PS is higher than the ones for CPS. This is due to the concentration of PO_5 and PO_6 units in PS system higher than the ones in CPS system. The P-O-P bond angle distribution in PS system is like the ones in CPS. This means that the P-O-P bond angle distribution is almost not been affected by CaO content. Figure 8 shows the O-Si-O and Si-O-Si bond angle distribution in PS and CPS systems. It shows that, the O-Si-O and Si-O-Si bond angle distribution in PS system is the same as in CPS. This means that the -O-Si-O- network structure is not dependent on CaO content. Figures 9 and 10 show the O-T-O and T-O-T bond angle distribution on PS and CPS systems. Results show that, the T-O-T bond angle distribution in PS and CPS systems is the same. The O-T-O bond angle

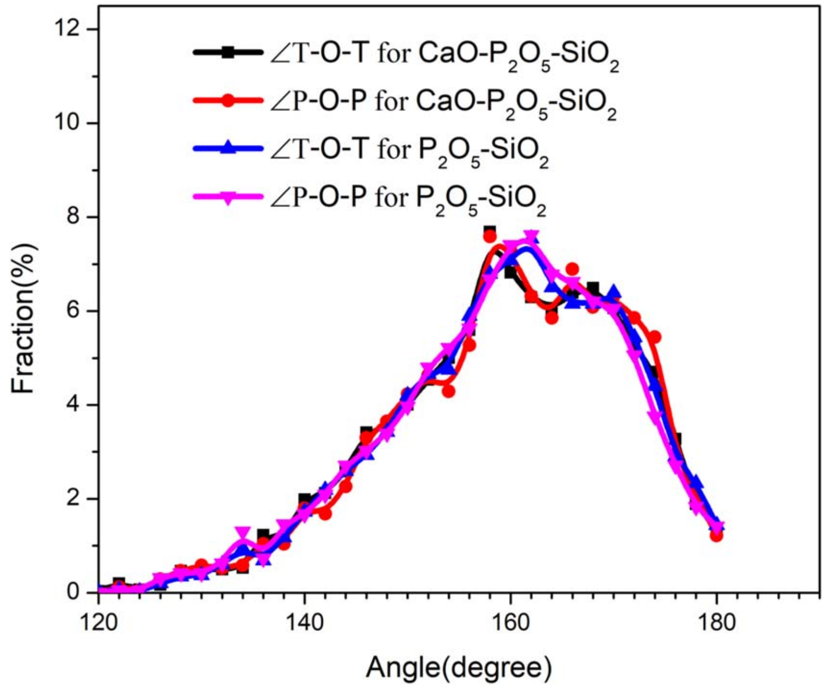

Figure 9. The T-O-T and P-O-P bond angle distribution in P_2O_5-SiO_2 and CaO-P_2O_5-SiO_2 systems.

Table 7. Distribution of Q^n units in CaO-P_2O_5-SiO_2 system (10 mol% CaO, 30 mol% P_2O_5 and 60 mol% SiO_2), here Q^n is the SiO_x, POx or TO_x (T = Si, P) with n bridging oxygens between Si-Si, P-P and T-T, respectively.

Q^n	Q^0	Q^1	Q^2	Q^3	Q^4	Q^5	Q^6	Total
SiO_4	27	171	231	141	38	—	—	608
SiO5	21	51	57	27	5	1	—	162
SiO_6	3	4	1	1	1	0	0	10
PO_4	184	273	138	23	2			620
PO_5	1	13	37	24	6	0		81
PO_6	0	0	11	24	32	9	3	79
TO_4	0	7	88	382	750			1227
TO_5	0	0	0	1	36	206		243
TO_6	0	0	0	0	0	6	83	89

Table 8. Distribution of Q^n units in P_2O_5-SiO_2 system (40 mol% P_2O_5 and 60 mol% SiO_2), here Q^n is the SiO_x, POx or TO_x (T = Si, P) with n bridging oxygens between Si-Si, P-P and T-T, respectively.

Qn	Q^0	Q^1	Q^2	Q^3	Q^4	Q^5	Q^6	Total
SiO4	58	194	188	83	20	0	0	543
SiO5	28	63	55	12	2	0	0	160
SiO6	6	7	2	1	1	0	0	17
PO4	88	251	236	95	12	0	0	682
PO5	1	10	40	54	47	4	0	156
PO6	0	0	17	28	47	22	8	122

distribution in PS and CPS is significantly different about the peak height. This reveals that, the SRO in PS and CPS is quite different. In other word, the CaO content strongly effects to the IRO of CPS. The Q^n distribution in PS and CPS is quite different. This means that, the CaO content affects strongly the Q^n distribution and the degree of polyamorphism of CPS system CaO.

4. Conclusion

The structure and network topology of PS and CPS have been studied systematically by molecular dynamics simulation and visual analysis method. Structure of PS and CPS is formed from TO_x (T = 4, 5, 6) coordination units. These units connect to each other via BOs forming network of TOx. The Ca^{2+} ions tend to locate nearby NBO or BO that connects between SiO_x and PO_x units. The network structure of PS and CPS systems consists of two networks: -O-P-O-P-O- and O-Si-O-Si-O- network. The Ca^{2+} ions tend to incorporate into network via BOs, mostly via BO(P). The structure of PS and CPS systems exhibits the structural and compositional heterogeneities. It forms the P-rich regions besides the Si-rich regions. In the CPS, it also forms the Ca-rich regions, this is also the Si-poor regions. Ca-rich regions tend to locate at boundary between PO_x and SiO_x-networks. The CaO content affects significantly the Q^n distribution and degree of polymerization of the network structure. The data about the structure of CPS and PS systems are the key information for research and development the bioactive material that bases on multicomponent oxide system.

Data availability statement

This study are available upon reasonable reques. The data that support the findings of this study are available upon reasonable request from the authors.

ORCID iDs

Nguyen Van Hong https://orcid.org/0000-0002-0097-9840
Nguyen Hoang Anh https://orcid.org/0000-0002-7504-5284
Mai Thi Lan https://orcid.org/0000-0002-2980-9132

References

[1] Stevensson B, Mathew R and Eden M 2014 Assessing the phosphate distribution in bioactive phosphosilicate glasses by 31P solid-state NMR and molecular dynamics simulations *J. Phys. Chem. B* **118** 8863–76

[2] Tilocca A 2011 Molecular dynamics simulations of a bioactive glass nanoparticle *J. Mater. Chem.* **21** 12660

[3] Tilocca A 2009 Structural models of bioactive glasses from molecular dynamics simulations *Proc. R. Soc.* **465** 1003–27

[4] Pedonea A, Cannillo V and Menziani, M C 2021 Toward the understanding of crystallization, mechanical properties and reactivity of multicomponent bioactive glasses, *Acta Materialia,* **213** 116977

[5] Fernandes H R, Gaddam A, Rebelo A, Brazete D, Stan G E and Ferreira J M F 2018 Bioactive glasses and glass-ceramics for healthcare applications in bone regeneration and tissue engineering, *Materials* **11** 2530

[6] Yu Y, Mathew R and Edén M 2018 Quantitative composition–bioactivity relationships of phosphosilicate glasses: bearings from the phosphorus content and network polymerization, *J. Non-Cryst. Solids* **502** 106–17

[7] Pratik Bhaskar *et al* 2020 Cooling rate effects on the structure of 45S5 bioglass: Insights from experiments and simulations, *J. Non-Cryst. Solids* **534** 119952

[8] Doweidar H 2009 Density–structure correlations in Na_2O–CaO–P_2O_5–SiO_2 bioactive glasses *J. Non-Cryst. Solids* **355** 577–80

[9] Kapoor S, Semitela Â, Goel A, Xiang Y, Du J, Lourenço A H, Sousa D M, Granja P L and Ferreira J M F 2015 Understanding the composition–structure–bioactivity relationships in diopside (CaO·MgO_2SiO_2)–tricalcium phosphate (3CaO·P_2O_5) glass system *Acta Biomater.* **15** 210–26

[10] Fábián M *et al* 2020 Network structure and thermal properties of bioactive (SiO_2-CaO-Na2O-P2O5) glasses *J. Mater. Sci.* **55** 2303–20

[11] Yaxian Z *et al* A modified random network model for P_2O_5– Na_2O–Al_2O_3–SiO_2 glass studied by molecular dynamics simulations *RSC Adv., 2021* **11** 7025–36

[12] Ibrahim M A *et al* 2020 Computational notes on the effect of (Li-Na-K) on calcium zinc phosphate oxide glasses *Biointerface Research in Applied Chemistry* **10** 6906–11

[13] Oliveira J M, Correia R N and Fernandes M H 2000 Effect of SiO_2 on amorphous phase separation of CaO-P_2O_5-SiO_2-MgO glasses *J. Non-Cryst. Solids* **273** 59 ±63

[14] Wang Z *et al* 2017 Structural investigation of phosphorus in CaO-SiO_2-P_2O_5 ternary glass *Metall Mater Trans* **48** 1139–48

[15] Hoppe U, Kranold R, Barz A, Stachel D, Neuefeind J and Keen D A 2001 Combined neutron and x-ray scattering study of phosphate glasses *J. Non-Cryst. Solids* **293–295** 158–68

[16] FitzGerald V 2007 A neutron and x-ray diffraction study of bioglass® with reverse monte carlo modelling *Adv. Funct. Mater.* **17** 3746–53

[17] Li D, Fleet M E, Bancroft G M, Kasrai M and Pan Y 1995 Local structure of Si and P in SiO_2-P_2O_5 and Na_2O-SiO_2-P_2O_5 glasses: a XANES study *J. Non-Cryst. Solids* **188** 181–9

[18] Mysen B O, Ryerson F J and Virgo D 1981 The structural role of phosphorus in silicate melts *Am. Mineral.* **66** 106–17

[19] Eckert H 2018 Structural characterization of bioactive glasses by solid state NMR *J. Sol-Gel Sci. Technol.* **88** 263–95

[20] de Oliveira Jr M, Aitken B and Eckert H 2018 Structure of P_2O_5–SiO_2 pure network former glasses studied by solid state NMR spectroscopy *J. Phys. Chem. C* **122** 19807–15

[21] Tilocca A 2007 Structure and dynamics of bioactive phosphosilicate glasses and melts from ab initio molecular dynamics simulations *Phys. Rev.* **76** 224202

[22] Tommaso D D, Ainsworth R I, Tang E and de Leeuw N H 2013 Modelling the structural evolution of ternary phosphate glasses from melts to solid amorphous materials *J. Mater. Chem. B* **1** 5054–66

[23] Tilocca A, de Leeuw N H and Cormack A N 2006 Shell-model molecular dynamics calculations of modified silicate glasses *Phys. Rev.* **73** 104209

[24] Wang Z, Cai S, Zhang M, Guo M and Zhang Z 2017 Structural investigation of phosphorus in CaO-SiO_2- P_2O_5 ternary glass *Metallurgical and Materials Transactions* **48** 1139–48

[25] Hoppe U, Kranold R, Stachel D, Barz A and Hannonb A C 2000 'Variation in P-O bonding in phosphate glasses -a neutron diffraction study' *Z. Naturforsch.* **55** 369–80

[26] Lee S K, Mun K Y, Kim Y-H, Lhee J, Okuchi T and Lin J-F 2020 Degree of permanent densification in oxide glasses upon extreme compression up to 24 GPa at room temperature *The Journal of Physical Chemistry Letters* **11** 2917–24

[27] Kim E J, Kim Y-H and Lee S K 2019 Pressure-induced structural transitions in Na–Li silicate glasses under compression *J. Phys. Chem.* **123** 26608–22

[28] Mathew R *et al* 2013 Direct probing of the phosphate-ion distribution in bioactive silicate glasses by solid-state NMR: evidence for transitions between random/clustered scenarios *Chem. Mater.* **25** 1877–85

[29] Wetherall K M, Pickup D M, Newport R J and Mountjoy G 2009 The structure of calcium metaphosphate glass obtained from x-ray and neutron diffraction and reverse Monte Carlo modelling *J. Phys. Condens. Matter* **21** 035109

[30] Stevensson B, Yu Y and Eden M 2018 Structure–composition trends in multicomponent borosilicate-based glasses deduced from molecular dynamics simulations with improved B–O and P–O force fields *Phys. Chem. Chem. Phys.* **20** 8192

[31] Montazeriana M, Zanottoa E D and Mauro J C 2020 Model-driven design of bioactive glasses: from molecular dynamics through machine learning *Int. Mater. Rev.* **65** 5

[32] Christie J K, Ainsworth R I, Ruiz Hernandez S E and de Leeuw N H 2017 Structures and properties of phosphate-based bioactive glasses from computer simulation: a review *J. Mater. Chem.* **5** 5297

[33] Fan G, Diao J, Jiang L, Zhang Z and Xie B 2015 Molecular dynamics analysis of the microstructure of the CaO-P_2O_5-SiO_2 slag system with varying P_2O_5/SiO_2 ratios *Mater. Trans.* **56** 655–60

[34] Belashchenko D K and Ostrovskii O I 2002 Computer simulation of noncrystalline ionic–covalent oxides CaO–P_2O_5 *Inorg. Mater.* **38** 146–53

[35] Diao* J, Ke Z, Jiang L, Zhang Z, Zhang T and Xie B 2017 Structural properties of molten CaO–SiO_2–P_2O_5–FeO System *High Temp. Mater. Proc.* **36** 871–6

[36] Bødker M L, Pedersen J B, Muñoz F, Mauro J C and Smedskjae M M Statistical mechanical model for the formation of octahedral silicon in phosphosilicate glasses *The American Ceramic Society* **105** 1031–8

[37] Lee S K, Lee A C and Kweon J J 2021 Probing medium-range order in oxide glasses at high pressure *J. Phys. Chem. Lett.* **12** 1330–8

[38] Leea S K, Kima Y-H, Chowc P, Xiaoc Y, Jic C and Shenc G 2018 Amorphous boron oxide at megabar pressures via inelastic x-ray scattering *PNAS* **115** 5855–60

[39] Kim E J, Kim,† Y-H and Lee S K 2019 Pressure-induced structural transitions in Na—Li silicate glasses under compression *J. Phys. Chem.* **123** 26608–22

[40] Kapoor S, Wondraczek L and Smedskjaer M M 2017 *Pressure-induced densification of oxide glasses at the glass transition *Front. Mater. Sec. Ceramics and Glass* **4** 1

[41] McKeown D A, Muller I S, Matlack K S and Pegg I L 2002 X-ray absorption studies of vanadium valence and local environment in borosilicate waste glasses using vanadium sulfide, silicate, and oxide standards *J. Non-Cryst. Solids* **298** 160–75

[42] Youngman R 2018 NMR spectroscopy in glass science: a review of the elements Materials 11, 476

[43] Bouty O, Delaye J M, Beuneu B and Charpentier T 2014 Modelling borosilicate glasses of nuclear interest with the help of RMC, WAXS, neutron diffraction and 11B NMR *J. Non-Cryst. Solids* **401** 27–31

[44] Yu Y, Stevensson B and Ed´en M 2019 The structural role of sodium in borosilicate, phosphosilicate, and borophosphosilicate glasses unveiled by solid-state NMR and MD simulations *J. Phys. Chem.* **123** 25816–32

[45] Lu X *et al* 2021 Effects of Al: Si and (Al + Na):Si ratios on the properties of the international simple glass *Structure, J. Am. Ceram. Soc.* **104** part II 183–207

[46] Benmore C J 2012 A review of high-energy x-ray diffraction from glasses and liquids *ISRN Mater. Sci.* **2012** 1–19

[47] Lu X, Ren M, Deng L, Benmore C J and Du J 2019 Structural features of ISG borosilicate nuclear waste glasses revealed from high-energy x-ray diffraction and molecular dynamics simulations *J. Nucl. Mater.* **515** 284–93

[48] Mastelaro V R and Zanotto E D 2018 X-ray absorption fine structure (XAFS) studies of oxide glasses-a 45-year overview Materials 11, 204

[49] Jollivet P, Calas G, Galoisy L, Angeli F, Bergeron B, Gin S, Ruffoni M P and Trcera N 2013 An enhanced resolution of the structural environment of zirconium in borosilicate glasses *J. Non-Cryst. Solids* **381** 40–7

[50] Lu X and Du J 2022 Effects of boron oxide on the structure, properties and bioactivities of bioactive glasses: A review *Journal of Non-Crystalline Solids: X* **16** 100118

[51] Ispas S, Benoit M, Jund P and Jullien R 2001 Structural and electronic properties of the sodium tetrasilicate glass Na 2 Si 4 O 9 from Classical and *Ab Initio* molecular dynamics simulations *Phys. Rev.*B **64** 214206

[52] Du J and Corrales L R 2006 Structure, dynamics, and electronic properties of lithium disilicate melt and glass *The J. of chem. phys.* **125** 114702

[53] Belonoshko A B, Lukinov T, Fu J, Zhao J, Davis S and Simak S I 2017 Stabilization of body-centred cubic iron under inner-core conditions *Nature Geosci* **10** 312–6

[54] Hafner J 2008 *Ab-Initio* simulations of materials using vasp: density-functional theory and beyond *J. of comput. chem.* **29** 2044–78

[55] Kresse G. and Furthmuller J. 2002 , Universität Wien, VASP-Guide

[56] Linfeng Ding *et al* 2020 Atomic structure of hot compressed borosilicate glasses *J. Am. Ceram. Soc.* **103** 6215–25

[57] Atila A, Ghardi E M, Ouaskit S and Hasnaoui A 2019 Atomistic insights into the impact of charge balancing cations on the structure and properties of aluminosilicate glasses *Phys. Rev.*B **100** 144109

[58] Zhang Q, Xue Z, Wang X and Xu D 2022 Molecular dynamics simulation of biomimetic biphasic calcium phosphate nanoparticles *J. Phys. Chem.* **126** 9726–36

[59] Achraf Atila E M G and Abdellatif Hasnaoui S O 2019 Alumina effect on the structure and properties of calcium aluminosilicate in the percalcic region: a molecular dynamics investigation *J. Non-Crystalline Solids* **525** 119470

[60] Achraf Atila S O and Hasnaoui A 2020 Ionic self-diffusion and the glass transition anomaly in aluminosilicates *Phys. Chem. Chem. Phys.* **22** 17205–12

[61] Zhiyu Xue X W and Xu D 2022 Molecular dynamic simulation of prenucleation of apatite at a type I collagen template: ion association and mineralization control *Phys. Chem. Chem. Phys.* **24** 11370–81

[62] Ouldhnini Y, Atila A, Ouaskitc S and Hasnaoui A 2021 Atomistic insights into the structure and elasticity of densified 45S5 bioactive glasses *Phys. Chem. Chem. Phys.* **23** 15292–301

[63] Atila A, Ouldhnini Y, Ouaskit S and Hasnaoui A 2022 Atomistic insights into the mixed-alkali effect in phosphosilicate glasses *Phys. Rev.* **105** 134101

[64] Tuheen M I and Du J 2022 Structural features and rare earth ion clustering behavior in lanthanum phosphate and aluminophosphate glasses from molecular dynamics simulations *J. Non-Cryst. Solids* **578** 121330

[65] Qian Y, Song B, Jin J, Prayogo G I, Utimula K, Nakano K, Maezono R, Hongo K and Zhao G 2022 *Ab initio* molecular dynamics simulation of structural and elastic properties of SiO_2–P_2O_5–Al_2O_3–Na_2O glass *J. Am. Ceram. Soc.* **105** 6604–15

[66] Ouldhnini Y, Atila A, Ouaskit S and Hasnaoui A 2022 Density-diffusion relationship in soda-lime phosphosilicate *J. Non-Cryst. Solids* **590** 121665

[67] Tilocca A, Cormack A N and de Leeuw N H 2007 The structure of bioactive silicate glasses: new insight from molecular dynamics simulations *Chem. Mater.* **19** 95–103

[68] Malavasi G and Pedone A 2022 The effect of the incorporation of catalase mimetic activity cations on the structural, thermal and chemical durability properties of the 45S5 Bioglass *Acta Mater.* **229** 117801

[69] Drewitt J W E 2021 Liquid structure under extreme conditions: high-pressure x-ray diffraction studies *J. Phys. Condens. Matter* **33** 503004 (32pp)

[70] Ghosh D B and Karki B B 2018 First-principles molecular dynamics simulations of anorthite ($CaAl_2Si_2O_8$) glass at high pressure *Phys. Chem. Minerals* **45** 575–87

[71] Drewitt J W E 2021 Liquid structure under extreme conditions: high-pressure x-ray diffraction studies *J. Phys. Condens. Matter* **33** 503004

[72] Kapoor S, Guo X, Youngman R E, Hogue C L, Mauro J C, Rzoska S J, Bockowski M, Jensen L R and Smedskjaer M M 2017 Network glasses under pressure: permanent densification in modifier-free Al_2O_3-B_2O_3-P_2O_5-SiO_2 systems *Phys. Rev. Applied* **7** 054011

[73] Miguel A, Salvadó and Pertierra P 2008 Theoretical study of P_2O_5 polymorphs at high pressure: hexacoordinated phosphorus *Inorg. Chem.* **47** 4884–90

[74] Nguyen Van Hong N T T H and Pham Khac Hung T I 2019 Pressure-induced structural change of CaO–Al_2O_3–SiO_2 melt: insight from molecular dynamics simulation *Mater. Chem. Phys.* **236** 121839

[75] Lan M T, Duong T T, Iitaka T and Van Hong N 2017 Computer simulation of CaSiO3 glass under compression: correlation between Si–Si pair radial distribution function and intermediate range order structure *Mater. Res. Express* **4** 065201

[76] Malavasi G *et al* 2013 New insights into the bioactivity of SiO_2–CaO and SiO_2–CaO–P_2O_5 sol–gel glasses by molecular dynamics simulations *J. Sol-Gel Sci. Technol.* **67** 208–19

[77] Thompson A P *et al* 2022 LAMMPS - a flexible simulation tool for particle-based materials modeling at the atomic, meso, and continuum scales *Computer Physics Communications (LAMMPS) CPC Library link to program files* **271** 108171

[78] Abyzov A S, Fokin V M, Yuritsyn N S, Rodrigues A M and Schmelzer J W P 2017 The effect of heterogeneous structure of glass-forming liquids on crystal nucleation *J. Non-Cryst. Solids* **462** 32–40

[79] Mai Thi Lan *et al* 2017 Network structure of SiO_2 and $MgSiO_3$ in amorphous and liquid States *Mater. Res. Express* **4** 035202

[80] Jürgen Horbach W K and Binder K 2001 Structural and dynamical properties of sodium silicate melts: an investigation by molecular dynamics computer s81]imulation *Chem. Geol.* **174** 87–101

[81] Ying Shi O, Gulbiten J, Neuefeind D, Ma A P, Song B, Wheaton M, Bauchy and Elliott S R 2020 Temperature-induced structural change through the glass transition of silicate glass by neutron diffraction *Phys. Rev.* **101** 134106

[82] Nhan N T and Hung P K 2020 New analysis characterizing the dynamics heterogeneity and microstructure in liquid silicates *J. Phys.: Conf. er* 1506012018 https://iopscience.iop.org/article/10.1088/1742–6596/1506/1/012018

[83] Van Hoang V 2007 Dynamical heterogeneity and diffusion in high-density $Al_2O_3 \cdot 2SiO_2$ melts *Physica B* **400** 278–86

[84] Benmore C J, Alderman O L G, Benmore S R, Wilke S K and Richard J K 2020 Weber small- and wide-angle x-ray scattering studies of liquid–liquid phase separation in silicate melts *ACS Earth Space Chem.* **4** 1888–94

[85] Michael Vogel and Glotzer S C 2004 Temperature dependence of spatially heterogeneous dynamics in a model of viscous silica *Phys. Rev.* **70** 061504